

## MHD mode localisation in the JET tokamak

B. Alper<sup>2</sup>, L. Barrera<sup>3</sup>, M. Baruzzo<sup>4</sup>, A. Botrugno<sup>1</sup>, P. Buratti<sup>1</sup>, L. Figini<sup>5</sup>, D.F. Howell<sup>2</sup>, C. Giroud<sup>2</sup>, E. De La Luna<sup>3</sup>, P. Piovesan<sup>4</sup>, O. Tudisco<sup>1</sup> and JET-EFDA contributors\*

JET-EFDA, Culham Science Centre, OX14 3DB, Abingdon, UK

<sup>1</sup>Associazione Euratom/ENEA sulla Fusione, CP 65-00044 Frascati, Rome, Italy

<sup>2</sup>Euratom/UKAEA Fusion Association, Culham Science Centre, Abingdon, OX14 3DB, UK

<sup>3</sup>Laboratorio Nacional de Fusión, Asociación EURATOM-CIEMAT, 28040, Madrid, Spain

<sup>4</sup>Consorzio RFX, EURATOM-ENEA Association, Corso Stati Uniti 4, 35127 Padova, Italy

<sup>5</sup>Istituto di Fisica del Plasma, Associazione EURATOM ENEA -CNR, Milano, Italy

### 1. Introduction

Two different methods for localising low-order rational  $q$  locations in the JET tokamak have been developed. Both are based on the radial localisation of magnetic islands, which corresponds to rational  $q = m/n$  values resonating with the island helicity. The island toroidal mode number  $n$  is determined without any ambiguity by a toroidal array of Mirnov coils while, since poloidal information in Mirnov coils is corrupted by plasma shape effects, the poloidal mode number  $m$  is inferred with the aid of preliminary raw information on the  $q$  profile from equilibrium reconstruction. These mode-localisation techniques are particularly useful in high-beta advanced tokamak scenarios, in which neoclassical tearing modes (NTMs) driven by density and temperature gradient perturbations are very frequently observed. In this paper both methods will be presented and their results will be compared.

### 2. Island localisation by frequency

This technique is based on the assumption that the island propagates at the ion diamagnetic frequency ( $\omega_{*pi} = -(n/eN)dP_i/d\psi$ ) in the frame with zero radial electric field. Frequency in the laboratory frame is then  $\omega = \omega_{*pi} + \omega_{ExB}$ . This assumption is supported by experimental [1, 2] and theoretical [3] studies, but it is not yet fully established; for this reason the technique needs validation by cross-checking with other ones.

$\omega_{ExB}$  is given by the radial momentum balance of carbon impurity; neglecting poloidal rotation

and density gradient,  $\omega_{ExB} = n\Omega_T - (n/6)dT_C/d\psi$ , with carbon temperature and rotation profiles as measured by Charge Exchange Spectroscopy. Assuming  $T_i = T_C$  and neglecting the

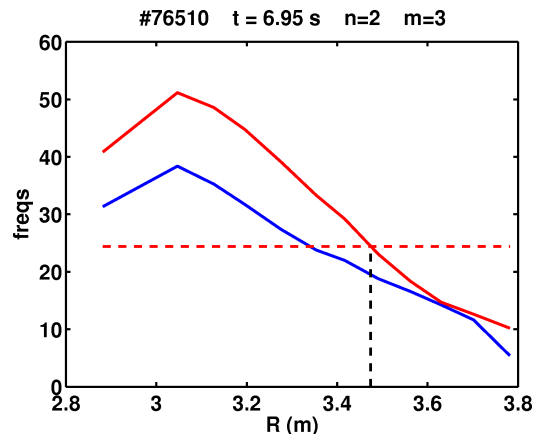


Figure 1.  $\omega_{ExB}$  (blue line) and  $\omega_{*pi} + \omega_{ExB}$  (red line) for a  $m/n = 3/2$  mode. Horizontal and vertical lines shows measured mode frequency and resulting mode location  $R_{n,m}$  respectively.

\* See the Appendix of F. Romanelli et al., Fusion Energy Conference 2008 (Proc. 22nd Int. FEC Geneva, 2008) IAEA, (2008)

density gradient in  $\omega_{pi}$ , frequency in the laboratory frame becomes  $\omega = n\Omega_T - (5n/6)dT_C/d\psi$ . Matching of the right hand side with frequency measured by fast magnetic coils gives island location  $R_{n,m}$  (Fig. 1). Several spectral lines can be followed in time, as shown in Fig. 2. A location signal is generated for each line by tracking the local spectral maximum. Measurement precision depends on fluctuations in CX data (mainly due to ELMs). Two more error sources arise from neglecting density gradient and using  $\Psi$  from unconstrained equilibrium reconstruction; both can be corrected by refining the analysis (see Sect. 4).

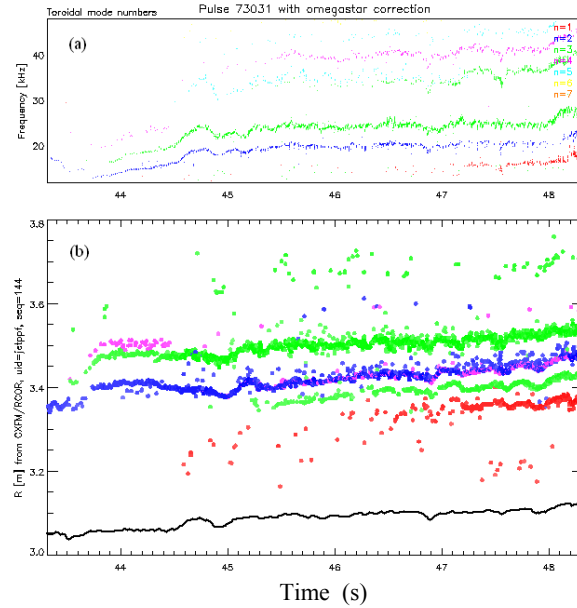


Figure 2. (a) Spectrogram of magnetic signals, with toroidal number shown in color code. (b) Mode locations in major radius for  $m/n=1/1$  (red),  $4/3$  (inner green points),  $3/2$  (blue),  $5/3$  (outer green points).

### 3. Island localisation by temperature oscillations

The technique is based on the observation that equilibrium perturbation by a rotating magnetic island induces a particular pattern in temperature profile oscillations [4], in such a way that coherence phase radial profile shows a  $\pi$ -jump whenever an island is crossed moving along the plasma radius. In order to detect the radial position of island chains, a time-frequency domain coherence technique [5] was implemented using two different diagnostic measurements, the signal from a fast magnetic pick up coil and the set of 48 signals from the ECE fast radiometer which measures the radial profile of electron temperature and its temporal fluctuations.

The approach starts from  $n$ -number analysis of magnetic signals, which assigns an  $n$ -number to each frequency bin and provides a basis to filter out the temperature oscillations which are not linked to the selected  $n$ -number perturbation. Then an automatic algorithm for mode tracking in the time-frequency domain is used to follow the frequency evolution for each  $n$  mode number. This procedure also gives the absolute amplitude of each mode in the magnetic signal. A calculation of the coherence amplitude and phase in Fourier space between the magnetic signal and each ECE channel is performed using Welch's method. The mode frequency provided by the tracking algorithm is used to calculate coherence just in the FFT

frequency bin of the mode, in order to increase signal to noise ratio and to reduce the computing time. The following step is an algorithm designed to find the radial position of phase jumps for each time slice and for each mode. Particular care was taken to discard low average coherence amplitude temporal frames ( $C < 0.4$ ) and couple of points too far one from each other ( $\delta_R > 10\text{cm}$ ). The

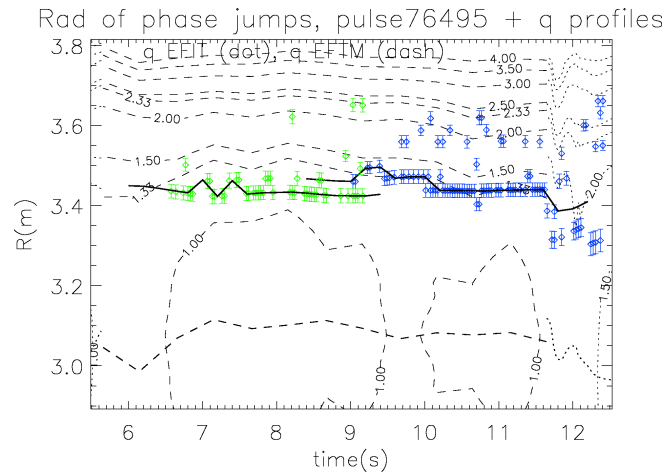


Figure 3. Mode locations for the 4/3 and 3/2 modes. Error bars represent half the distance between channels that enclose the  $\pi$ -phase jump.

last step is an algorithm for extracting a signal with mode radius as a function of time. For this aim a tracking algorithm is used, similar to the one used to detect mode frequency in the magnetic signals, which follows in time the maximum value in space-time density of phase jump points. More than one iteration of this process is used to find NTMs position, in this way multiple tracks for each mode can be found, till a maximum number of three [6]. Again particular care was taken to avoid picking up phase jumps due to noise, using a cross check with coherence cross spectrum at that radius, to find a fluctuation amplitude sensibly larger than noise value. All this software can be run in unattended mode.

Fig. 3 shows the results of the analysis, with detected phase jumps represented by dots with error bars and the tracked mode location over plotted to phase jump points as a black line. Error bars are estimated as half of the distance between the two neighbouring channels that enclose the phase jump. The main systematic uncertainty of this technique arises in the determination of the radial positions of ECE channels, which depends

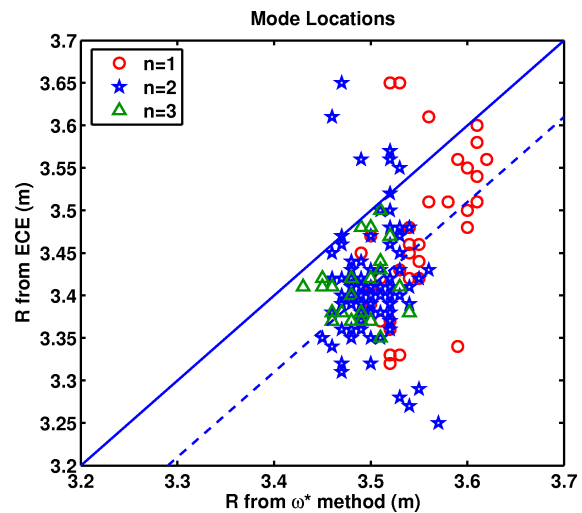


Figure 4. Comparison between locations from mode frequency and from  $T_e$  oscillations for  $m/n=2/1$ ,  $3/2$  and  $4/3$  modes. Identity corresponds to the blue solid line. The dashed line is shifted by 9 cm.

on the accuracy of magnetic field profile reconstruction including plasma current and diamagnetic contributions. At low magnetic field also the refraction can be relevant and its effects on the island position has been evaluated by a ray-tracing code.

#### 4. Results

Fig. 4 shows a comparison between radial locations from frequency and ECE methods, for  $n = 1, 2, 3$  mode numbers. On average, locations from ECE are 9 cm more internal than the ones from mode frequency. ECE vs. MSE comparison gives better agreement, with a shift of about 5 cm. Fig. 5 shows a comparison between locations from mode frequency and from MSE diagnostic. In this case there is agreement on average, but still with significant spread, in particular at low  $R_{MSE}$ . The black star shows the effect of applying to the most discrepant point (connected by the black curve) a recursive correction for  $\psi$  and an improved fit to the temperature gradient. Still a significant discrepancy remains, which has to do either to errors in the MSE  $q$ -profile, or to some effect neglected in mode analysis (like poloidal rotation, while inclusion of density

gradient would increase the discrepancy). Fig. 6 shows that a large discrepancy arises if ion diamagnetic drift is completely ignored. In summary, comparison between MSE and mode frequency data shows that the assumption of mode rotation at the ion diamagnetic frequency is substantially correct. A systematic discrepancy with ECE data is found, which could be reconciled with a 3% correction to the total equilibrium magnetic field.

#### References

- [1] P.C. de Vries and R.J.E. Jaspers, EPS 1997
- [2] R.J. La Haye Phys. Plasmas **10** (2003) 3644
- [3] R. Fitzpatrick and F.L. Waelbroeck, Phys. Plasmas **15**, 012502 (2008)
- [4] R. Fitzpatrick, Phys. Plasmas **2** (3), 1995
- [5] P. Welch, IEEE transactions vol.15, issue 2 ,70-73, 1967
- [6] M. Baruzzo et al., this conference, P5.170

Acknowledgement. This work, supported by the European Communities under the EURATOM/ENEA contract of Association, was carried out within the framework of the European Fusion Development Agreement. The views and opinions expressed herein do not necessarily reflect those of the European Commission.

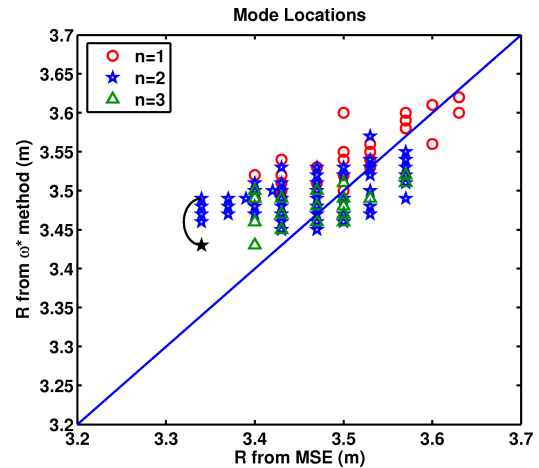


Figure 5.  $q$  locations from mode frequency and from MSE diagnostic for  $m/n= 2/1, 3/2$  and  $4/3$ . Identity corresponds to the blue solid line.

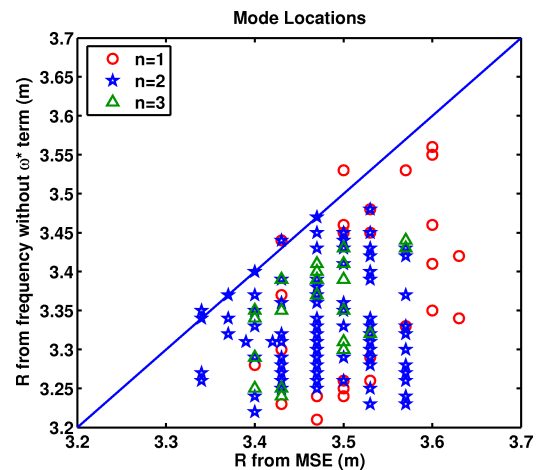


Figure 6. Rational  $q$  locations from mode frequency without ion diamagnetic drift and from MSE diagnostic. Identity corresponds to the blue line.